Proceedings of the 17th World Congress
The International Federation of Automatic Control
Seoul, Korea, July 6-11, 2008

# Two sensor based $H_\infty$ control of a piezoelectric tube scanner ⋆

**I. A. Mahmood, K. Liu and S. O. R. Moheimani**

*School of Electrical Engineering and Computer Science,*
*The University of Newcastle, Callaghan, NSW 2308, Australia*
*(Tel: +61 2 49216030; e-mail: Reza.Moheimani@newcastle.edu.au)*

**Abstract:** The performance of a feedback-controlled piezoelectric tube scanner is limited by its inherent nonlinear properties such as hysteresis and creep, its mechanical resonance modes and its displacement sensor bandwidth and associated noise properties. Capacitive sensors have emerged as the displacement sensor of choice in piezoelectric tube scanners. Resolution of a capacitive sensor is largely determined by its bandwidth and noise density which is typically in the order of 20 pm/$\sqrt{\text{Hz}}$ for a $\pm 100$ $\mu$m range. Consequently, to achieve sub-nanometer resolution, the sensor's bandwidth needs to be made small. Achieving satisfactory tracking performance using a low-bandwidth displacement sensor is a challenging task. To improve the bandwidth, the piezoelectric strain voltage induced in the electrode opposite to the actuating electrode is used as a secondary measurement. A two-sensor-based $H_\infty$ controller is designed and implemented on a prototype piezoelectric tube nanopositioning system. The tube is driven by a charge amplifier to reduce the hysteresis. Experimental results demonstrate a significant increase in the tracking bandwidth due to the use of the additional sensor.

## 1. INTRODUCTION

Piezoelectric transducers have been used in a wide range of applications such as vibration control of flexible structures, Pota et al. (2002), active noise control, Shields et al. (1997) and also in scanning probe microscopes (SPM). The term SPM is a name given to a group of microscopes such as scanning tunneling microscope (STM), atomic force microscope (AFM) and other similar devices which use a probe to develop images of material surfaces over a range of several 100 $\mu$m down to 10 pm, Meyer et al. (2004).

Application of the piezoelectric tube in SPMs was first reported in Binnig and Smith (1986) for the use in the STM. In a SPM, the piezoelectric tube is used to either move the probe or the sample in a raster pattern in order to scan the entire region of interest. A raster scanning is normally performed by moving the piezoelectric tube along the x-axis in forward and reversed directions (horizontal scanning), and then moving the piezoelectric tube along the y-axis in a small step to reach the next line (frame scanning) for another horizontal scanning, Mironov (2004). During the forward-pass of horizontal scanning, the surface topographic information gathered by the probe is stored for image processing. The speed of a piezoelectric scanner is largely determined by the scanning frequency of horizontal scanning.

The positioning precision of the piezoelectric tube can be adversely affected by vibrations and non-linearities exhibited by the piezoelectric material such as hysteresis and creep, Croft et al. (2001). The main source of vibrations is induced vibrations due to excitation of the lightly-damped first resonant mode by higher harmonics of the horizontal scanning frequency. In practice, in order to minimize the induced vibrations, the horizontal scanning frequency is limited to 1/100th of the first resonance frequency of the tube. As for the non-linearities, the adverse effects of hysteresis and creep can be reduced by limiting the scanning range and operating time of the piezoelectric tube respectively. The above mentioned limitations restrict the use of the piezoelectric tube scanner for high speed and long scanning range operations.

In general, the control techniques for piezoelectric tube scanner can be classified into two groups, feedforward and feedback control schemes. An attractive feature of feedforward control scheme is that this method does not require any additional sensors for implementation. In Croft et al. (2001), model-based inversion approach was used to compensate for positioning distortions caused by creep, hysteresis and induced vibrations. A low-order feedforward controller was presented in Schitter and Stemmer (2001) to suppress the lateral oscillation of a piezoelectric tube scanner. The feedforward controller was designed using $H_\infty$ method such that the system was not excited at frequencies around the first resonance of the piezoelectric tube scanner. However, it was noted in Croft et al. (2001) and Schitter and Stemmer (2001) that the performance of feedforward control schemes rely on an accurate model of the piezoelectric tube scanner.

A number of feedback control schemes have been proposed for the control of piezoelectric tube scanners. Two feedback controllers, lag-lead and $H_\infty$ controllers were designed and implemented in Tamer and Dahleh (1994). Here, a non-contacting inductive sensor was used to measure the lateral displacement of the tube. It was shown that, both controllers successfully compensated the effect of creep and hysteresis. However, only the $H_\infty$ controller was

⋆ This research was supported by Australian Research Council Center of Excellence for Complex Dynamic Systems and Control.

effective in damping out the high-frequency disturbances. In Daniele et al. (1999), the loop shaping procedure was used in designing feedback controllers using optical sensors to track a raster pattern. Their results show significant reductions in tracking error and cross coupling when employing feedback control. Feedback control schemes can be designed to be robust to modeling error and achieve good tracking performance.

The performance of feedback control schemes is limited by the bandwidth and noise properties of the position sensor. In this work, we propose a control scheme to increase the bandwidth of a feedback-controlled piezoelectric tube scanner by using the piezoelectric strain voltage induced in the electrode opposite to the actuating electrode as a secondary tip deflection measurement in addition to the primary tip deflection measurement obtained from a low-bandwidth capacitive sensor. Simultaneous use of the two sensors allows the bandwidth of the closed-loop system to be increased substantially without increasing the noise level due to the capacitive sensor measurements. An $H_\infty$ control design approach was employed to design a dual-loop feedback controller that utilizes both measurements at two different frequency ranges to track a triangular wave input. The resulting system has a closed-loop bandwidth of 310 Hz, which is more than three times the bandwidth afforded by the capacitive sensor.

The remainder of the paper is arranged as follows. Section 2 provides a description of the experimental setup. Modeling and identification of the system transfer functions are presented in Section 3. Control schemes are devised in Section 4. In Section 5, experimental results are presented to illustrate the effectiveness of the proposed control schemes. Finally, conclusions are drawn in Section 6.

## 2. SYSTEM DESCRIPTION

The piezoelectric tube used in this paper is a cylindrical tube made of piezoelectric material plated with a layer of electrode on the inner and outer surfaces of the tube. The inner electrode is continuous and grounded. The outer layer electrode is segmented into four equal sized electrodes and referred to individually as $+x$, $-x$, $+y$ and $-y$ electrodes. The physical dimensions of the tube are given in Fig. 1(a). The piezoelectric tube is housed in a circular aluminum enclosure to protect it from external disturbances. An aluminum cube is glued to the top of the tube to serve as a sample holder and also to provide the capacitive sensors with flat surfaces so that the tip deflection of the tube can be measured accurately. The capacitive sensors are fixed at the right angle to the cube surface in the x-axis and y-axis by using nylon screws as shown in Fig. 1(b). The root-mean-square (RMS) noise density of the capacitive sensors were measured in Fleming et al. (2007) to be 17.5 pm/$\sqrt{\text{Hz}}$. By setting its bandwidth to 100 Hz, the RMS noise or the resolution of the capacitive sensors are set to 0.175 nm.

The tip deflection can be doubled by applying equal and opposite sign inputs to the electrodes opposite to each other. In this work, the forward and reversed motions of the tube in the x-axis are achieved by applying a triangular wave input to the $+x$ electrode only. The

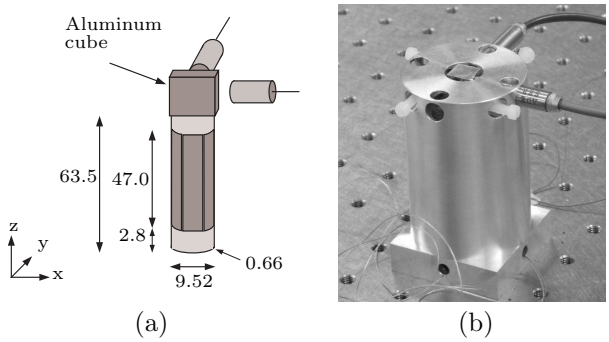


Fig. 1. (a) Piezoelectric tube dimensions in mm, (b) The piezoelectric tube is housed in a circular aluminum enclosure.

opposite electrode $-x$ is used as a secondary sensor to measure the tip deflection. When the tube deflects, the piezoelectric strain voltage induced in the $-x$ electrode is found to be proportional to the tip deflection over a certain frequency range. The transfer function from the strain voltage to the output of an instrumentation amplifier is a first-order high-pass filter, Moheimani and Fleming (2006), due to the capacitive nature of the source impedance. The high-pass filter can be expressed as,

$$G_{hp}(s) = \frac{s}{s + \frac{1}{R_{in}C_p}} \tag{1}$$

where $R_{in}$ is the input impedance of the voltage measuring instrument and $C_p$ is the capacitance of the piezoelectric tube. A gain $k_a$ is used to adjust the sensitivity of the $-x$ electrode such that it is equal to the sensitivity of the capacitive sensors. The proposed control scheme was implemented using a charge amplifier, Fleming and Moheimani (2005), in order to reduce the adverse effect of hysteresis. The charge amplifier has a constant gain of 68 nC/volt. A dSPACE DS1103 controller board was used for real-time controller implementation and a sampling frequency of 15 kHz was used in order to avoid aliasing.

## 3. SYSTEM IDENTIFICATION

The following frequency response functions (FRFs) are determined using a dual channel HP35670A spectrum analyzer,

$$G_{v_x u_x}(i\omega) = \frac{v_x(i\omega)}{u_x(i\omega)} \tag{2}$$

$$G_{c_x u_x}(i\omega) = \frac{c_x(i\omega)}{u_x(i\omega)} \tag{3}$$

where $u_x$ is the input voltage to the charge amplifier, $v_x$ is the induced piezoelectric strain voltage and $c_x$ is the output voltage of the capacitive sensor. The subscript $x$ denotes that the actuation and measurements are performed along the x-axis. A band-limited random noise signal (1 to 1601 Hz) was generated using the spectrum analyzer and applied to the charge amplifier as the input, $u_x$. The corresponding outputs $v_x$ and $c_x$ were also recorded using the same device. The input-output data was processed to generate the FRFs of (2) and (3) in a non-parametric form as illustrated in Fig. 2.

It can be seen from Fig. 2 that $G_{v_x u_x}(i\omega)$ includes a high-pass filter transfer function with cutoff frequency of about

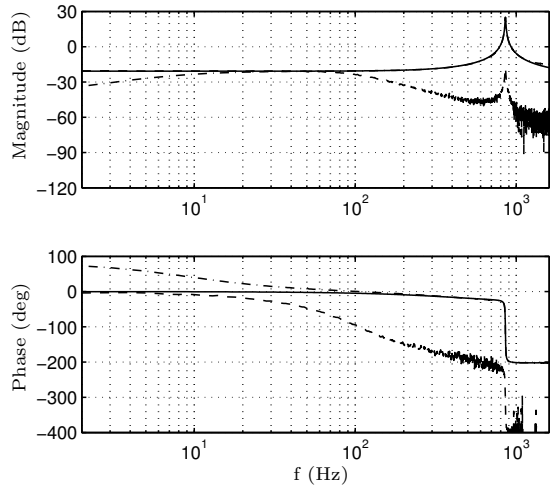


Fig. 2. Open-loop frequency response of $G_{v_x u_x}(i\omega)$ (dashed dots), $G_{c_x u_x}(i\omega)$ (dashed) and the identified model $G_{y_x u_x}(s)$ (solid).

9 Hz. The high-pass filter transfer function results in a phase-lead and heavy attenuation of the strain voltage. Thus, the strain voltage cannot be used as a reliable tip deflection measurement at low frequencies. Nevertheless from about 20 Hz and onwards, the strain voltage provides an excellent signal that can be used to estimate the tip deflection and also the dynamics of the piezoelectric tube. As for $G_{c_x u_x}(i\omega)$, its frequency response includes a low-pass filter transfer function with cutoff frequency of 100 Hz. Thus, the capacitive sensor can be used to measure the tip deflection below 70 Hz with acceptable accuracy. After this frequency, $G_{c_x u_x}(i\omega)$ starts to roll off considerably.

In this work instead of fitting separate transfer functions to $G_{v_x u_x}(i\omega)$ and $G_{c_x u_x}(i\omega)$, a new FRF was formed by using the low frequency range of the $G_{c_x u_x}(i\omega)$ data and the high frequency range of the $G_{v_x u_x}(i\omega)$ data. The new FRF corresponds to the true deflection of the tip, $y_x$. A second order model was fitted to the new FRF data. The following model was found to be a good fit as illustrated in Fig. 2,

$$G_{y_x u_x}(s) = \frac{-0.06s^2 - 342.8s + 2.654 \times 10^6}{s^2 + 49.47s + 2.895 \times 10^7} \qquad (4)$$

The high-pass and the low-pass filter transfer functions corresponding to $G_{v_x u_x}(i\omega)$ and $G_{c_x u_x}(i\omega)$ respectively are fitted with the following models

$$G_{hp}(s) = \frac{s}{s + 55.29} \qquad (5)$$

$$G_{lp}(s) = \frac{3.948 \times 10^5}{s^2 + 888.6s + 3.948 \times 10^5}. \qquad (6)$$

## 4. CONTROLLER DESIGN

The target of the design is to obtain a controller to achieve good damping ratio for the resonant mode of the tube scanner, to reduce the effect of hysteresis and to achieve higher bandwidth tracking performance. This is to be done using measurements obtained from both capacitive sensor,

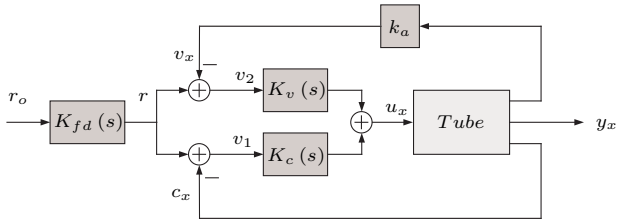


Fig. 3. Two degrees of freedom control block diagram.

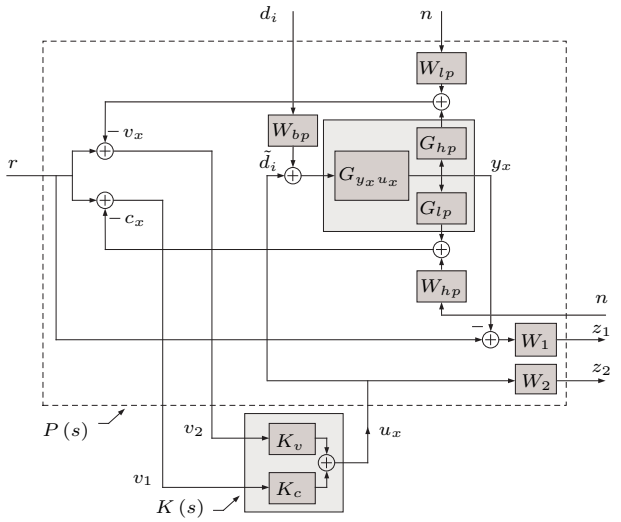


Fig. 4. Feedback control block diagram with weighting functions.

and the strain voltage signal. These two measurements complement each other since the former is reliable at low frequencies, including at DC, and the latter is accurate at high frequencies. The proposed control diagram is shown in Fig. 3 where a two degree of freedom controller scheme is to be synthesized. The control structure consists of the feedforward controller, $K_{fd}(s)$ and the feedback compensators, $K_v(s)$ and $K_c(s)$.

We will first design the feedback controllers $K_v(s)$ and $K_c(s)$. Fig. 4 illustrates the feedback control block diagram with weighting function diagram of the system. The problem can be cast into the standard $H_\infty$ controller design framework as shown in Fig. 5. The exogenous inputs are defined as $w = [\, r \;\; d_i \;\; n \,]^\top$ and the exogenous output as $z = [\, z_1 \;\; z_2 \,]^\top$, where $r$ is the reference signal to be tracked; $d_i$ represents vibrations modeled as input disturbance, and $n$ represents sensor noise; $u_x$ is the control signal and $v$ is the measured output. From Fig. 4, we have $z_1 = W_1(r - G_{y_x u_x}(u_x + W_{bp} d_i))$, and $z_2 = W_2 u_x$. The control signal is $u_x$ and the measured output is $v = [\, v_1 \;\; v_2 \,]^\top$, where $v_1 = r - (G_{y_x u_x}(u_x + W_{bp} d_i) G_{lp} + W_{hp} n)$ and $v_2 = r - (G_{y_x u_x}(u + W_{bp} d_i) G_{hp} + W_{lp} n)$.

To achieve good damping ratio, we introduce a disturbance $d_i$ at the plant input and try to minimize $T_{y_x d_i}$, the transfer function from $d_i$ to actual output $y_x$. The weighting function $W_{bp}$ considers the resonance mode to be damped at around 850Hz as shown in Fig. 2 and is chosen as,

$$W_{bp}(s) = \frac{1793s}{s^2 + 1793s + 2.893 \times 10^7}. \qquad (7)$$

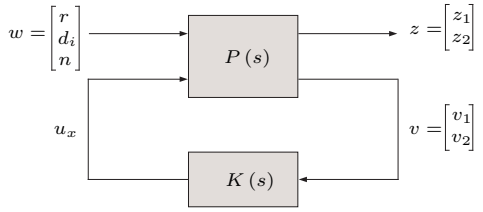


Fig. 5. General feedback control configuration.

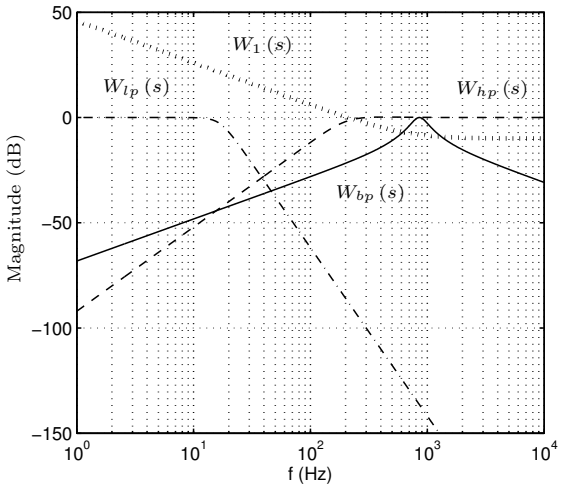


Fig. 6. Weighting functions.

The capacitive sensor is noisy at high frequencies and the piezoelectric strain voltage signal is distorted at low frequencies. The controller is designed to utilize the capacitive sensor for tracking low-frequency signals, and the strain voltage for tracking signals that contain higher frequency components. This is achieved by introducing the two weighting functions $W_{hp}$ and $W_{lp}$, as shown in Fig. 4,

$$W_{lp}(s) = \frac{1.262 \times 10^8}{(s^2 + 195.9s + 1.124 \times 10^4)} \times \frac{1}{(s^2 + 81.13s + 1.124 \times 10^4)} \quad (8)$$

and

$$W_{hp}(s) = \frac{s^2}{s^2 + 1571s + 1.579 \times 10^6}. \quad (9)$$

Furthermore, $W_2 = 0.1$ is used to impose a constraint on the control signal. This is to avoid excessively large control signals that could saturate the actuator.

The weighting function $W_1$ is incorporated to enforce good tracking performance. The inverse of this transfer function can be considered as desired sensitivity transfer function $T_{er}$, the transfer function from reference signal $r$ to tracking error $e = r - y_x$. $W_1$ is chosen as

$$W_1(s) = \frac{0.3162s + 1257}{s + 1.257}. \quad (10)$$

Fig. 6 illustrates the main weighting functions. The achieved sensitivity function is plotted against the desired transfer function in Fig. 7. Fig. 8 illustrates the frequency response of the feedback controller $K_c(s)$ and $K_v(s)$.

The final stage of the controller synthesis involves designing the feedforward controller $K_{fd}(s)$ to shape the reference signal based on the achieved closed-loop frequency response, $T_{y_x r}(s)$. The feedforward controller should be chosen such that:

$$K_{fd}(s) \approx T_{y_x r}^{-1}(s). \quad (11)$$

Since the reference signal $r_o(t)$ is known and $T_{y_x r}(jw)$ can be measured in advance, the shaped reference signal $r(t)$ can be obtained off-line as shown in Fig. 9.

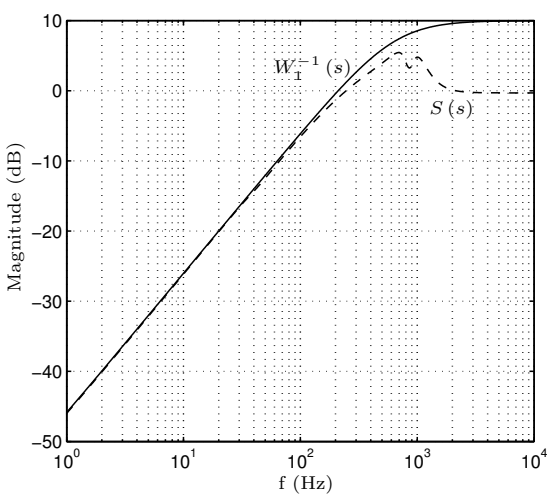


Fig. 7. Sensitivity functions, desired (solid) and achieved (dashed).

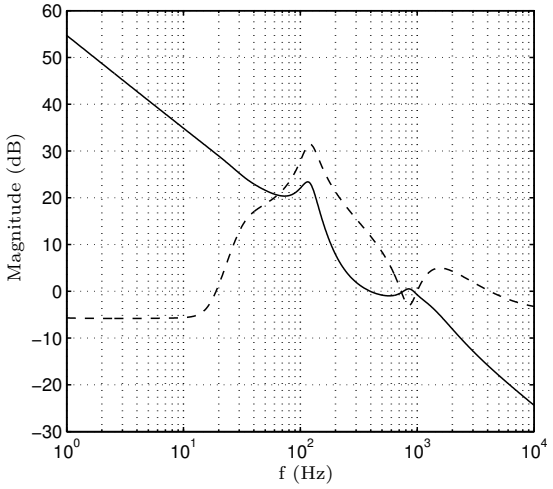


Fig. 8. Frequency response of the designed controllers $K_c(s)$ (solid) and $K_v(s)$ (dashed).

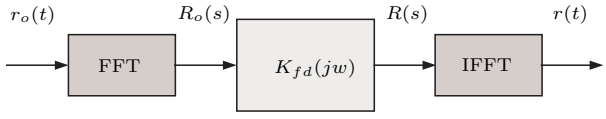


Fig. 9. Procedure to obtain shaped reference $r(t)$

## 5. RESULTS

This section presents experimental results obtained from the control schemes proposed in this paper. In order to measure the true deflection $y_x$, a high bandwidth (10 kHz)

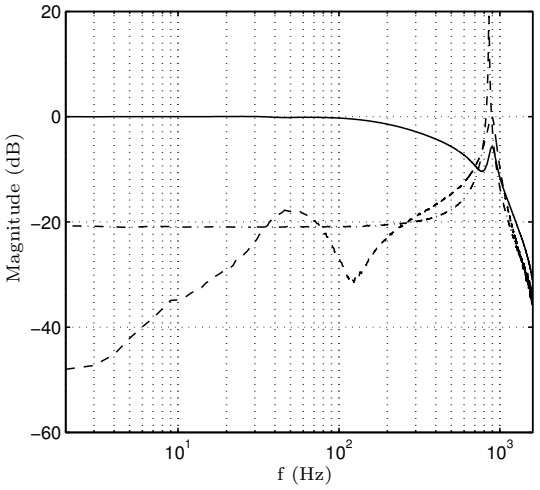


Fig. 10. Experimentally obtained frequency response of $T_{y_x r}(i\omega)$ (solid), $T_{y_x \tilde{d}_i}(i\omega)$ (dashed) and $G_{y_x u_x}(i\omega)$ (dashed dots).

capacitive sensor was used in all tests. The performance of the feedback controllers $K_c(s)$ and $K_v(s)$ were evaluated first by measuring the system closed-loop responses using the spectrum analyzer. In Fig. 10, the closed-loop frequency responses, $T_{y_x r}(i\omega)$ and $T_{y_x \tilde{d}_i}(i\omega)$ are plotted along with the open-loop frequency response, $G_{y_x u_x}(i\omega)$. By inspecting the frequency response of $T_{y_x r}(i\omega)$ we conclude that the closed-loop system has a bandwidth of 310 Hz. This is about three times higher than the bandwidth of the capacitive sensor alone. A damping of 20 dB at the first resonant mode is evident from the frequency response of $T_{y_x \tilde{d}_i}(i\omega)$. Note that the frequency response also shows that the closed-loop system is insensitive to low-frequency input disturbances. Hence, the closed-loop system will perform in a satisfactory manner in presence of low-frequency vibrations and disturbances.

The presence of hysteresis in the prototype nanopositioner was investigated by applying a 5 Hz sinusoidal signal to the piezoelectric tube and measuring its deflection in open-loop. A single-tone low frequency signal was chosen here in order to avoid excitation of the first resonant mode of the tube. The tube was made to deflect large distance ($\pm$ 3.0$\mu$m) so that the presence of hysteresis could be clearly observed. The effects of hysteresis were evaluated when the tube was driven by a voltage amplifier and a charge amplifier. For each case the corresponding input signal and the tip deflection were recorded. Figs. 11 (a) and (b) illustrate the plots of tip deflection versus input signal for voltage and charge, respectively. A clear reduction of hysteresis can be observed when the tube is driven by the charge amplifier. In order to measure the reductions, we quantified the hysteresis in terms of the maximum input (or output) hysteresis given as a percentage of the full scale as given in Salapaka et al. (2002). The quantified hysteresis are tabulated in Table 1 and clearly demonstrate the immediate benefit of driving the tube with a charge amplifier. Although the hysteresis is not reduced to an absolute zero, it is made so small that the actuator can effectively be considered a linear device.

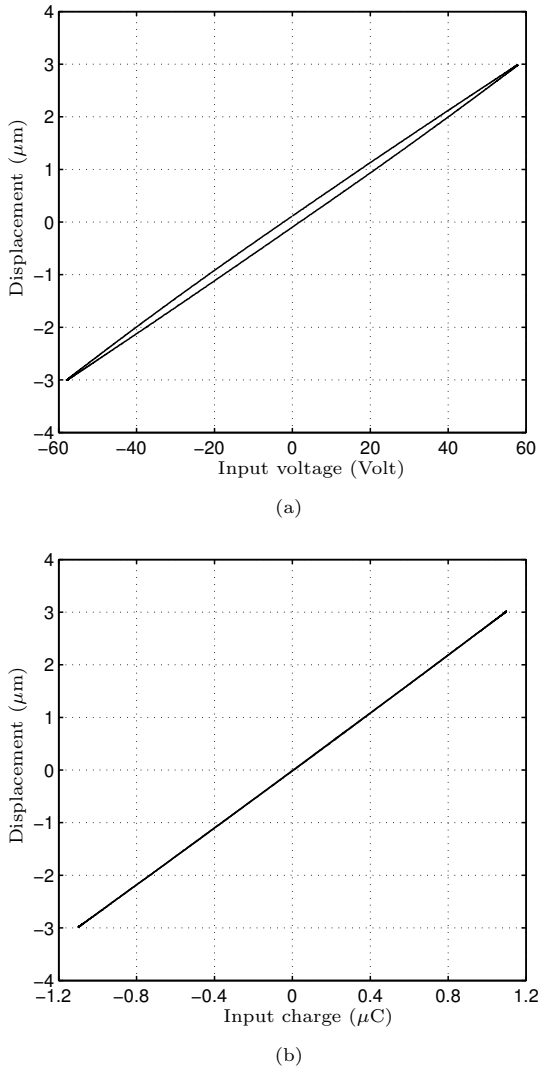


Fig. 11. Hysteresis plot of 5 Hz open-loop scan using (a) voltage amplifier and (b) charge amplifier.

Table 1. Numerical quantification of hysteresis

| Configurations | Max. output hysteresis | Max. input hysteresis |
|---|---|---|
| Voltage amp. | 207.50 nm (3.5%) | 4.12 volt (3.6%) |
| Charge amp. | 11.60 nm (0.19%) | 4.60 nC (0.21%) |

Figs. 12 (a) and (b) illustrate the time responses of the tube's tip deflection due to a 19 Hz triangular wave input. The tube was driven by a charge amplifier in open-loop and closed-loop respectively. The plot in Fig. 12(a) illustrates that motion of the tip is badly affected by the induced vibrations in open-loop. However, in closed-loop, Fig. 12 (b) shows the designed controllers damped all the induced vibrations and provide excellent tracking of the 19 Hz triangular wave input. It can be observed that, there is a phase shift of 6 degrees between the reference signal and the tip deflection. By using the shaped triangular wave input, see Fig. 12 (c), the phase shift is reduced to 3 degrees.

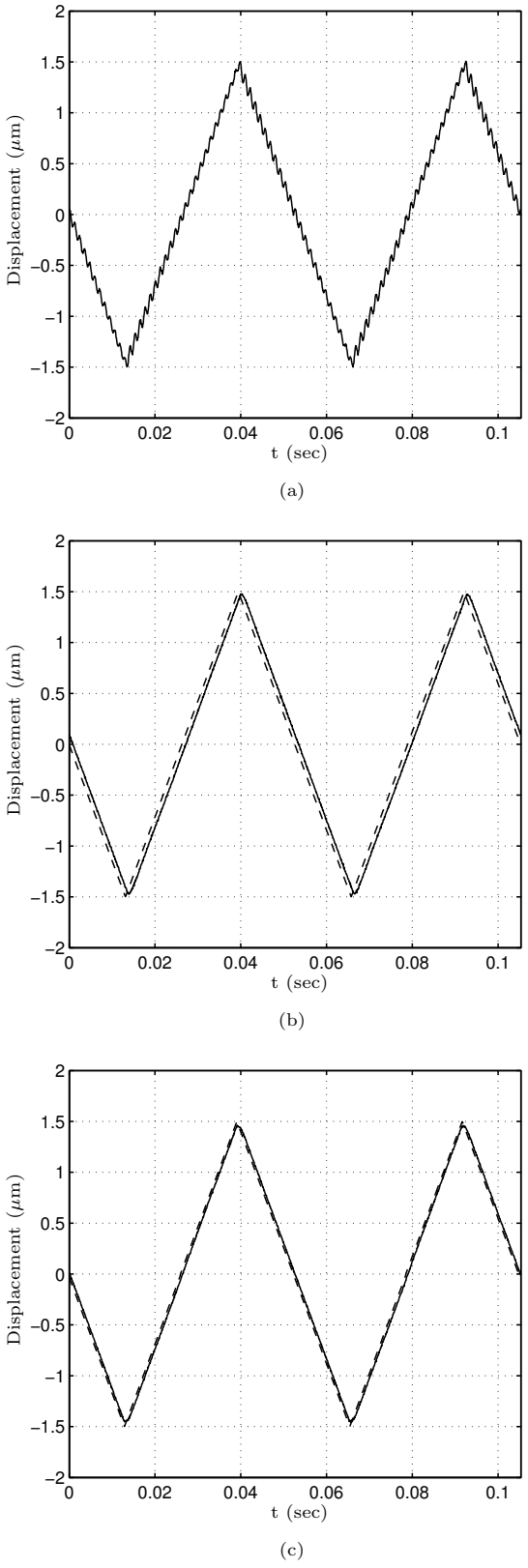


Fig. 12. Time response plot of 19 Hz scan in (a) open-loop, (b) closed-loop with triangular wave input and (c) closed-loop with shaped triangular wave input.

## 6. CONCLUSION

In this paper, we presented a systematic design method based on $H_\infty$ control approach in designing controllers for two feedback loops such that the controllers operate at two different frequency ranges simultaneously. The designed controllers successfully eliminate the effect of the hysteresis and damp the first resonant mode of the tube. Experimental results illustrate that the use of the piezoelectric strain voltage as a secondary measurement allows the closed-loop system bandwidth to be increased more than three times the bandwidth of the displacement sensor.

## REFERENCES

H. R. Pota, S. O. R. Moheimani, and M. Smith. Resonant controllers for smart structures. *Smart Materials and Structures*, vol. 11, pages 1–8, 2002.

W. H. Shields, J. Ro, and A. M. Baz. Control of sound radiation from a plate into an acoustic cavity using active piezoelectric-damping composites. *Proc. of SPIE Smart Structures and Materials: Mathematics and Control in Smart Structures*, SPIE vol. 3039, pages 70–90, 1997.

E. Meyer, H. J. Hug, R. Bennewitz. *Scanning Probe Microscopy: The Lab on a Tip.* Spring-Verlag, Berlin Heidelberg, 2004.

G. Binnig and D. P. E. Smith. Single-tube three-dimensional scanner for scanning tunneling microscopy. *Review of Scientific Instrument*, vol. 57(8), pages 1688 – 1689, August, 1986.

V. L. Mironov. *Fundamentals of Scanning Probe Microscopy.* Nizhniy Novgorod, 2004.

D. Croft, G. Shed and S. Devasia. Creep, Hysteresis, and Vibration Compensation for Piezoactuators: Atomic Force Microscopy Application. *Journal of Dynamic systems, Measurement, and Control*, vol. 123, pages 35–43, 2001.

G. Schitter and A. Stemmer. Identification and open-loop tracking control of a piezoelectric tube scanner for high-speed scanning-probe microscopy. *IEEE Transaction on Control System Technology*, vol. 12(3), pages 449–454, 2004.

N. Tamer and M. Dahleh. Feedback control of piezoelectric tube scanners. *Proc. of the 33rd Conference on Decision and Control*, pages 1826–1830, 1994.

A. Daniele, S. Salapaka, M. V. Salapaka, and M. Dahleh. Piezoelectric scanners for atomic force microscopes: design of lateral sensors, identification and control. *Proc. of the American Control Conference*, pages 253–257, 1999.

A. J. Fleming, A. Wills and S. O. R. Moheimani. Sensor fusion for improved control of piezoelectric tube scanners. *IEEE Transaction on Control System Technology*, (Accepted 2007).

S. O. R. Moheimani and A. J. Fleming. *Piezoelectric transducers for vibration control and damping.* Spring-Verlag, London, 2006.

A. J. Fleming and S. O. R. Moheimani. A grounded load charge amplifier for reducing hysteresis in piezoelectric tube scanners. *Review of Scientific Instrument*, vol. 76(7), 2005.

S. Salapaka, A. Sebastian, J. P. Cleveland and M. V. Salapaka. High bandwidth nano-positioner: a robust control approach. *Review of Scientific Instrument*, vol. 73(9), 2002.